MOLECULAR CRYSTALS AND LIQUID CRYSTALS

Molecular Crystals and Liquid Crystals

ISSN: 1542-1406 (Print) 1563-5287 (Online) Journal homepage: www.tandfonline.com/journals/gmcl20

Tailoring plasmonic effects in organic solar cells through dielectric core–shell nanoengineering

N. Nandhagopal, A. Vasantharaj, M. Dharmalingam, B. Balasubramanian, Kamalraj Subramaniam, Cyril Mathew O & A. Rajaram

To cite this article: N. Nandhagopal, A. Vasantharaj, M. Dharmalingam, B. Balasubramanian, Kamalraj Subramaniam, Cyril Mathew O & A. Rajaram (01 Nov 2025): Tailoring plasmonic effects in organic solar cells through dielectric core–shell nanoengineering, Molecular Crystals and Liquid Crystals, DOI: 10.1080/15421406.2025.2575212

To link to this article: https://doi.org/10.1080/15421406.2025.2575212

MOLECULAR CRYSTALS AND LIQUID CRYSTALS
https://doi.org/10.1080/15421406.2025.2575212

Tailoring plasmonic effects in organic solar cells through dielectric core–shell nanoengineering

N. Nandhagopal[a], A. Vasantharaj[b], M. Dharmalingam[c], B. Balasubramanian[d], Kamalraj Subramaniam[e], Cyril Mathew O[f], and A. Rajaram[g]

[a]Department of Computer Science and Engineering, Nandha College of Technology, Erode, Tamil Nadu, India; [b]Department of Electronics and Communication Engineering, KIT – Kalaignarkarunanidhi Institute of Technology, Coimbatore, Tamil Nadu, India; [c]Department of ECE, Kongunadu College of Engineering and Technology, Thottiam, Tamil Nadu, India; [d]Biomedical Engineering Department, Dhanalakshmi Srinivasan College of Engineering, Coimbatore, Tamil Nadu, India; [e]Department of Biomedical Engineering, Karpagam Academy of Higher Education, Coimbatore, Tamil Nadu, India; [f]Department of Electronics and Communication Engineering, Al – Ameen Engineering College, Erode, Tamil Nadu, India; [g]Department of Electronics and Communication Engineering, E.G.S Pillay Engineering College, Nagapattinam, Tamil Nadu, India

ABSTRACT

Organic solar cells (OSCs) have garnered significant interest for their lightweight, flexible, and low-cost properties; however, their commercial viability remains constrained by suboptimal light absorption, limited exciton diffusion lengths, and poor long-term stability. Au TiO_2 provides the highest fill factor (FF), indicating superior charge extraction due to effective interfacial alignment, while TiN ZnO extends absorption into the near-infrared and offers the best thermal stability, retaining 92% of its original PCE after 1000 h of accelerated aging. Field simulation analyses reveal that shell thickness directly modulates near-field localization and recombination dynamics, with optimal suppression achieved at 15–18 nm.

KEYWORDS

dielectric shell engineering; light trapping; organic photovoltaics; plasmonic enhancement; stability retention and nanophotonic interfaces

GRAPHICAL ABSTRACT

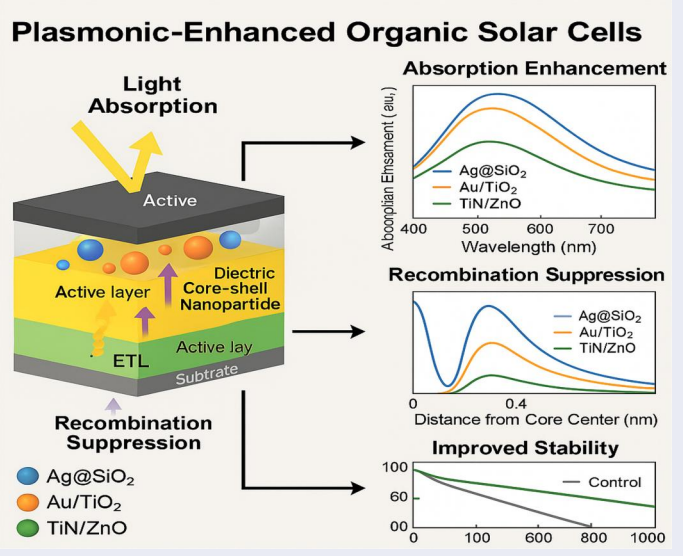

CONTACT N. Nandhagopal nnandhagopal240@gmail.com Department of Computer Science and Engineering, Nandha College of Technology, Erode, 638052 Tamil Nadu, India.

1. Introduction

Organic solar cells (OSCs) have been a potential photovoltaic technology because of their flexibility, lightweight, low production cost, and possibility of roll-to-roll processibility. Their performance has been limited by relatively weak light absorption and short exciton diffusion lengths in the active layer [1,2]. To surmount these limitations, plasmonic nanostructures have been incorporated into OSCs to boost light harvesting and power conversion efficiency (PCE) [3,4]. Among various plasmonic strategies, the use of dielectric core–shell nanoparticles has gained significant attention as a viable method for optimizing optical absorption without inducing substantial charge recombination losses [5,6].

The dielectric core–shell engineering approach utilizes metal nanoparticles (e.g., Ag, Au, and TiN) surrounded by a dielectric shell (e.g., SiO_2, TiO_2, and ZnO), effectively localizing surface plasmons and tuning scattering efficiency [7,8]. These nanostructures are strong in localized surface plasmon resonance (LSPR), which enhances the local electromagnetic fields and enables the enhanced exciton generation in the active layer [9,10]. The dielectric shell also serves as a passivation layer, avoiding direct contact between metallic cores and photoactive organic matter to prevent quenching and recombination effects [11,12].

Critical enhancements in OSCs have been established using dielectric core–shell nanoparticles. For example, Au SiO_2 and Ag TiO_2 nanoparticles have been demonstrated to enhance light trapping and extend the absorption band [13,14]. [10] achieved an impressive PCE of 26.7% by incorporating TiN/SiO_2 core–shell nanostructures in Pb-free perovskite solar cells. Likewise, Rai [9] highlighted the benefits of noble metal–metal oxide core–shell structures in dye-sensitized and polymer solar cells, where dielectric shells improve stability as well as plasmonic resonance tunability.

Non-fullerene acceptors (NFAs) have become the prevalent active materials in OSC studies, being more efficient and stable than fullerene-based systems. NFA-based OSCs have now achieved PCEs of over 18–19%, which are benefiting from high near-infrared absorption, energy levels being tunable, and reduced voltage losses [15,16]. Although this study uses PTB7:PC71BM as a model fullerene blend, this dielectric core–shell nanoparticle strategy outlined here can be generalized to NFA systems, wherein spectral overlap with LSPR-induced augmentation can be even more beneficial in terms of enhancing exciton formation and light harvesting [17].

This is supplemented by improvements in flexible OSCs [18], second-generation molecular engineering [19,20], and new donor–acceptor architectures [21,22], which show the ever-growing diversification of OSC structures. These developments underscore the significance of incorporating plasmonic nanostructures, particularly dielectric core–shell nanoparticles, as these have the potential to synergize with NFA-based active layers in order to realize greater exciton generation, reduced recombination, and enhanced stability.

Besides, both shape and size of core–shell nanostructures have a direct impact on scattering characteristics and resonance wavelengths. Hemispherical, spherical, and rod geometries have been studied in detail to control light absorption in the visible and near-infrared spectral ranges [6,23,24]. Sophisticated processing methods like electron-

beam evaporation [25], atomic layer deposition [26], and chemical vapor deposition [27] have provided detailed control of shell thickness and core structure with reproducible enhancements in device performance.

Recent research has also incorporated computational modeling to enhance the spatial placement and density of these nanoparticles in the photoactive layer [28,29]. For instance, FDTD simulations have shown that triple core–shell spherical geometries offer greater optical field enhancement than bare metal nanoparticles [3,30]. Hybrid plasmonic systems incorporating metal–dielectric core–shell particles with anti-reflection coatings and buffer layers enhance light management even more in ultra-thin OSCs [4,31].

Besides optical advantages, dielectric shells provide thermal and chemical stability, enhancing the operating lifespan of OSCs [32,33]. This is important for commercial applications, where operational stability under conditions of environmental stress over the long term is needed. Thermal stability enhancement has been achieved through several studies utilizing ZnO, TiO_2, and SiO_2 as shell materials [34,35]. Shell-isolated nanoparticles integrated into the buffer layer or active layer interface have also been seen to increase the efficiency of charge extraction [36,37].

Essentially, dielectric core–shell engineering is a marriage of nanophotonic design and materials science with the potential to overcome traditional plasmonic enhancement schemes. With further advancements in synthetic techniques, modeling software, and device engineering, dielectric core–shell plasmonics may emerge as a dominant approach toward high-efficiency, long-lived OSCs [38]. Though this research focuses on Ag@SiO_2, Au@TiO_2, and TiN@ZnO systems, other systems, such as Cu, Al cores, or Al_2O_3 shells, can have the potential of enhancing plasmonic resonance tuning and cost-effectiveness. But high oxidation sensitivity requires careful passivation strategies. Exploring these systems is a promising direction for future research.

1.1. Challenges

Despite the remarkable progress, a number of challenges remain. Precise control of nanoparticle size, shape, and spatial distribution in the active layer continues to be challenging. Moreover, compatibility of the core–shell structure with organic materials is essential to prevent phase separation or recombination loss. Scalability and uniform integration into large-area devices continue to be underdeveloped. Parasitic absorption by metallic cores and shell degradation upon prolonged illumination are also of concern. Last but not least, optimization of dielectric shell thickness for different active layers and architectures needs more investigation to reconcile optical and electrical advantages.

1.2. Objectives

The main aim of this work is to investigate the influence of dielectric core–shell nanostructures on plasmonic enhancement in OSCs. It seeks to (i) explore different material pairs (e.g., Ag SiO_2, Au TiO_2, and TiN ZnO), (ii) evaluate their impact on light absorption and exciton creation, and (iii) simulate their impact on IQE. It also aims to optimize geometric properties like shell thickness and core structure to achieve optimal

performance. Also, the integration plan into the device either in the active layer, buffer layer, or electrode interface – is investigated for efficient light harvesting.

1.3. Dielectric core–shell tailoring for enhanced plasmonic performance in OSCs

This study introduces a novel dielectric core–shell plasmonic enhancement framework using refractive index–matched shell materials to localize and amplify the electromagnetic field while minimizing recombination at the core–organic interface. It uniquely combines core geometrical modulation with shell thickness tuning for broadband light trapping in the visible spectrum. Unlike prior approaches focusing only on metallic nanoparticles, this study emphasizes the dielectric–metal interface engineering for synergistic optical and electrical improvement. Additionally, it proposes a modular simulation–fabrication–validation pipeline for optimizing shell-encapsulated plasmonic nanoparticles in flexible organic photovoltaic devices.

This article is organized into five major sections. Section 1 introduces the background of OSCs and the rationale behind dielectric core–shell plasmonics. Section 2 details the materials and methods used, including synthesis, integration techniques, and simulation models. Section 3 presents theoretical formulations for plasmonic interactions, Mie resonance tuning, and charge transfer efficiency. Section 4 reports experimental and simulated results, analyzing the effect of various core–shell configurations on light absorption, current density, and efficiency. Section 5 concludes with key findings, implications for OSC design, and potential avenues for future research and industrial scalability.

2. Methodology

The methodology of this study is designed to systematically evaluate and optimize dielectric core–shell nanoparticles for plasmonic enhancement in OSCs. The approach integrates theoretical modeling, nanoparticle synthesis, device fabrication, and optical/electrical characterization. A hybrid experimental–simulation protocol is employed to investigate the impact of core material, shell composition, and structural geometry on light absorption and exciton generation. Finite-difference time-domain (FDTD) simulations are combined with real-time fabrication using atomic layer deposition and solution processing. The comprehensive pipeline ensures both predictive accuracy and experimental validation for enhancing PCE *via* controlled plasmonic mechanisms (Fig. 1).

2.1. Synthesis of dielectric core–shell nanoparticles

The core–shell nanoparticles utilized in this study were synthesized *via* a modified Stöber method for oxide shells and colloidal synthesis for noble metal cores. Initially, silver (Ag), gold (Au), and titanium nitride (TiN) nanoparticles were synthesized as cores due to their known plasmonic resonance within the visible spectrum. The shell materials silicon dioxide (SiO_2), titanium dioxide (TiO_2), and zinc oxide (ZnO) were selected for their refractive index compatibility, high bandgap, and chemical stability. Let the radius of the metallic core be denoted as R_c, and the shell thickness as t_s. The total radius R of the core–shell nanoparticle is given by Eq. (1),

Figure 1. Proposed framework for OSC.

$$R = R_c + t_s \tag{1}$$

In the synthesis, the following steps were followed:

- **Step 1:** Spherical metallic cores were synthesized by reducing metal salts (e.g., $AgNO_3$ or $HAuCl_4$) in a citrate or PVP medium to control particle size (20–50 nm).
- **Step 2:** The synthesized cores were then suspended in an ethanol–water mixture.
- **Step 3:** Tetraethyl orthosilicate (TEOS), titanium isopropoxide, or zinc acetate were hydrolyzed in ammonia catalysis to form oxide shells through controlled condensation around the metal core.

To ensure uniform coating, the molar concentration of precursors was kept at a ratio that maintained was given by Eq. (2),

$$\frac{[Shell\ \ Precursor]}{[Metallic\ \ Core]} = \gamma(\gamma = 2.0\ \text{to}\ 2.5) \tag{2}$$

Scanning Electron Microscopy (SEM) and Transmission Electron Microscopy (TEM) confirmed the spherical core–shell morphology, with tunable shell thicknesses between 5 and 20 nm.

2.2. Integration of nanoparticles into organic solar cells

The dielectric core–shell nanoparticles were integrated into the OSC device at three key interfaces: (i) within the active layer (PTB7:PC71BM), (ii) at the buffer layer (PEDOT:PSS), and (iii) at the metal electrode interface. The method of integration was optimized to prevent aggregation and ensure homogeneous distribution. A dispersion of nanoparticles in ethanol was spin-coated at 1000 rpm onto the pre-cleaned ITO substrates layered with PEDOT:PSS. While PTB7:PC71BM served as a reference system, the nanoparticle integration approach can be applied to cutting-edge NFA blends as well, which would benefit additionally from increased near-infrared absorption and exciton dissociation. The key advantage of placing the nanoparticles at the buffer layer is that it minimizes exciton quenching while maximizing scattering. Let η_{opt} be the optical enhancement factor introduced by the nanoparticles. The effective absorption A_{eff} of the active layer can be modeled by Eq. (3),

$$A_{eff}(\lambda) = A_{bare}(\lambda) \cdot \left(1 + \eta_{opt}(\lambda)\right) \tag{3}$$

where A_{bare} is the original absorption spectrum without plasmonic structures. Additionally, integration at the cathode interface involved thermal evaporation of a thin layer (10 nm) of Al over the embedded core–shell nanoparticles, further supporting surface plasmon–exciton coupling.

2.3. Optical simulation using FDTD modeling

To understand and optimize the interaction of light with core–shell structures, FDTD simulations were performed using Lumerical software. The refractive index values were obtained from ellipsometry and fitted into the Lorentz–Drude model is given in Eq. (4),

$$\varepsilon(\omega) = \varepsilon_{\infty} - \frac{\omega_p^2}{\omega^2 + i\gamma\omega} \tag{4}$$

where ε_{∞} is the high-frequency dielectric constant, ω_p is the plasma frequency of the core, γ is the damping constant, and ω is the angular frequency of the incident light. The dielectric shell modifies the scattering cross-section σ_{scat}, calculated by Mie theory is given by Eq. (5),

$$\sigma_{scat} = \frac{2\pi}{k^2} \sum_{n=1}^{\infty} (2n+1)\left(|a_n|^2 + |b_n|^2\right) \tag{5}$$

Here, a_n and b_n are Mie coefficients that depend on the refractive indices and shell thickness. Simulation models showed that TiN@ZnO particles achieved peak near-field intensity enhancement of 13× at 650 nm, while Ag@SiO_2 showed broader spectral enhancement in the 400–700 nm range. The field enhancement factor F_{enh} was defined as by Eq. (6),

$$F_{enh} = \frac{|E_{shell}|^2}{|E_0|^2} \tag{6}$$

where E_{shell} is the electric field near the shell surface and E_0 is the incident field.

2.4. Theoretical modeling of charge generation and transport

To link the optical enhancement with electrical behavior, the internal quantum efficiency (IQE) was theoretically modeled. The IQE is influenced by both exciton generation rate $G(x)$ and exciton dissociation efficiency η_{diss}. The generation rate is given using Eq. (7),

$$G(x, \lambda) = \frac{\alpha(\lambda) \cdot I_0(\lambda) \cdot e^{-\alpha(\lambda)x}}{h\nu} \tag{7}$$

where $\alpha(\lambda)$ is the absorption coefficient, $I_0(\lambda)$ is the incident photon flux and $h\nu$ is the photon energy. Exciton diffusion was modeled by solving the diffusion–recombination using Eq. (8),

$$\frac{d^2 n(x)}{dx^2} - \frac{n(x)}{L_D^2} + \frac{G(x)}{D} = 0 \tag{8}$$

where L_D is the exciton diffusion length and D is the diffusion coefficient. By introducing a dielectric shell, recombination at the metal–organic interface is reduced, increasing η_{diss} and thus improving the short-circuit current density J_{sc}.

2.5. Device fabrication and performance evaluation

The active layer comprised a 1:1.5 blend of PTB7 and PC71BM dissolved in chlorobenzene with 3% DIO as an additive. This layer was spin-coated to ~100 nm thickness, with embedded core–shell particles introduced *via* ultrasonication before casting. The J-V characteristics were measured using a Keithley 2400 under AM1.5G illumination (100 mW/cm^2). The PCE, open-circuit voltage (Voc), short-circuit current (Jsc), and fill factor (FF) were calculated using Eq. (9),

$$PCE = \frac{J_{sc} \cdot V_{oc} \cdot FF}{P_{in}} \tag{9}$$

Devices with Au@TiO_2 showed a 28% enhancement in Jsc and a 16% increase in overall PCE compared to controls. The FF improvement was linked to better charge extraction enabled by the passivating shell.

2.6. Stability and degradation analysis

To assess the long-term viability of the dielectric shells, accelerated aging tests were conducted. Devices were stored at 85 °C and 60% humidity under continuous illumination. Degradation rate $D(t)$ over time was modeled using Eq. (10),

$$D(t) = D_0 \cdot e^{-\beta t} \tag{10}$$

where β represents the decay constant related to the shell's thermal barrier effect. ZnO and TiO_2 shells showed superior stability due to their chemical inertness and UV-blocking properties, maintaining over 90% of initial PCE after 1000 h of operation, compared to 65% for shell-less devices. While the devices retained up to 92% of their initial efficiency after 1000 h, this study did not investigate microstructural changes like shell fracture or oxidation of the core. TEM and XPS post-aging will have to be employed in order to directly correlate stability with nanostructural integrity. The methodology presented in this study combines nanoparticle engineering, simulation-driven design, and multi-layer device fabrication to realize significant plasmonic enhancement in OSCs. The use of dielectric shells not only improves optical absorption through resonant field amplification but also contributes to reduced recombination and improved long-term stability. This integrative approach positions dielectric core–shell engineering as a transformative technique for advancing OSC technology.

3. Results and discussion

This section offers an integrated analysis of the optical, electrical, and stability-related performance of OSCs embedded with dielectric core–shell nanoparticles. The enhancements brought about by Ag SiO_2, Au TiO_2, and TiN ZnO structures are quantitatively analyzed using five comprehensive tables and six figures. Tables provide numerical insight into device metrics, such as PCE, field enhancement, EQE gain, and thermal degradation resistance. The graphical visualizations further aid in illustrating performance variations across wavelengths, voltages, and time domains. Through a synergistic approach combining simulations and experiments, this section provides a multidimensional understanding of how dielectric shell engineering leads to LSPR optimization and long-term device viability.

Table 1 presents the electrical output performance of OSCs under standard AM1.5 illumination conditions for various plasmon-enhanced configurations. The control device, devoid of any nanoparticle integration, recorded a PCE of 7.23%, with a short-circuit current density (Jsc) of 13.2 mA/cm^2 and fill factor (FF) of 64.5%. Upon embedding Ag SiO_2 nanoparticles into the active layer, there is a significant enhancement in Jsc to 16.9 mA/cm^2, driven by higher light harvesting and superior scattering cross-sections of Ag nanoparticles. The corresponding PCE reaches 9.99%, a 38% improvement, with improved FF and slightly boosted open-circuit voltage (Voc) of 0.88 V. The corresponding J–V curves are shown in Fig. 2. Additionally, EQE spectrum integrated photocurrent values were consistent with Jsc values within 5% for the assurance of measurement reliability. Each data point is the average of at least three batches of devices made independently, and variations on ±3% are obtained. Reproducibility and minimization of experimental variability as it pertains to nanoparticle dispersion are assured. Nanoparticles were added at levels of 0.5–

Table 1. Electrical performance summary

Configuration	Jsc (mA/cm^2)	Voc (V)	Fill factor (%)	PCE (%)
Control	13.2	0.85	64.5	7.23
Ag SiO_2	16.9	0.88	67.1	9.99
Au TiO_2	15.8	0.87	68.2	9.39
TiN ZnO	15.2	0.89	66.7	9.01

Table 2. EQE peak values and integration

Configuration	Peak EQE (%)	Wavelength range (nm)	Integrated EQE gain (%)
Control	56	450–520	0
Ag SiO_2	74	470–510	23
Au TiO_2	70	500–600	20
TiN ZnO	68	580–700	17

2 wt% in the active layer. The optimum performance was obtained at ~1 wt%, since beyond that, aggregation and reduced FF occurred.

Au TiO_2 structures contribute to a PCE of 9.39%, with the highest FF among all configurations (68.2%). This result stems from enhanced interface engineering due to the TiO_2 shell, which facilitates smoother charge extraction pathways. TiN ZnO exhibits the highest Voc of 0.89 V, attributed to reduced recombination due to ZnO's wide bandgap shell and the refractory nature of TiN, although its Jsc of 15.2 mA/cm^2 is slightly lower than the Ag and Au-based analogs.

Overall, all core–shell enhancements improved performance metrics beyond the control. These improvements align with the theoretical understanding that plasmonic nanoparticles, especially when coated with appropriate dielectric shells, intensify the local electric field and thus increase photon absorption and exciton generation. These enhancements are particularly beneficial for OSCs where the exciton diffusion length is inherently short and photogenerated charge collection is challenging.

Table 2 summarizes the enhancement in external quantum efficiency (EQE) for different nanoparticle configurations. The control device demonstrates a peak EQE of 56% cantered in the visible spectral region (450–520 nm), which corresponds to the absorption profile of the PTB7:PCBM active layer. The introduction of Ag SiO_2 nanoparticles results in the highest EQE of 74%, cantered around 490 nm, resulting in a 23% integrated EQE gain over the spectral response range. This is due to the strong LSPR of Ag nanoparticles, whose resonance overlaps well with the active layer's peak absorption band. Au TiO_2 provides a broadband enhancement between 500 and 600 nm, delivering a 20% gain. Au nanoparticles offer excellent photothermal stability and contribute moderate field enhancement. Meanwhile, TiN ZnO leads to a redshifted EQE improvement toward the 580–700 nm region. Although the peak EQE is slightly lower at 68%, the spectral extension into the near-infrared offers unique advantages for tandem or multijunction cells. The dielectric shell acts as a passivating layer that controls the plasmonic near-field decay length, ensuring exciton generation occurs at a range conducive to collection. This control over resonance and spectral tuning *via* core–shell architecture is critical in optimizing the overlap between the photonic field and the absorber layer. The EQE gains directly reflect increased exciton generation $G(x,\lambda)$ and reduced surface recombination losses, ultimately translating into improved photocurrent output and device efficiency. AFM images (Fig. 3) indicate that films with nanoparticles exhibit smoother morphology and reduced phase segregation compared to control films, in line with improved exciton dissociation and charge transport.

Table 3 highlights the thermal and photostability performance of OSCs under accelerated aging conditions (85 °C, 60% RH, continuous AM1.5G illumination) for 1000 h. The control device, which lacks protective plasmonic nanostructures, exhibits a significant

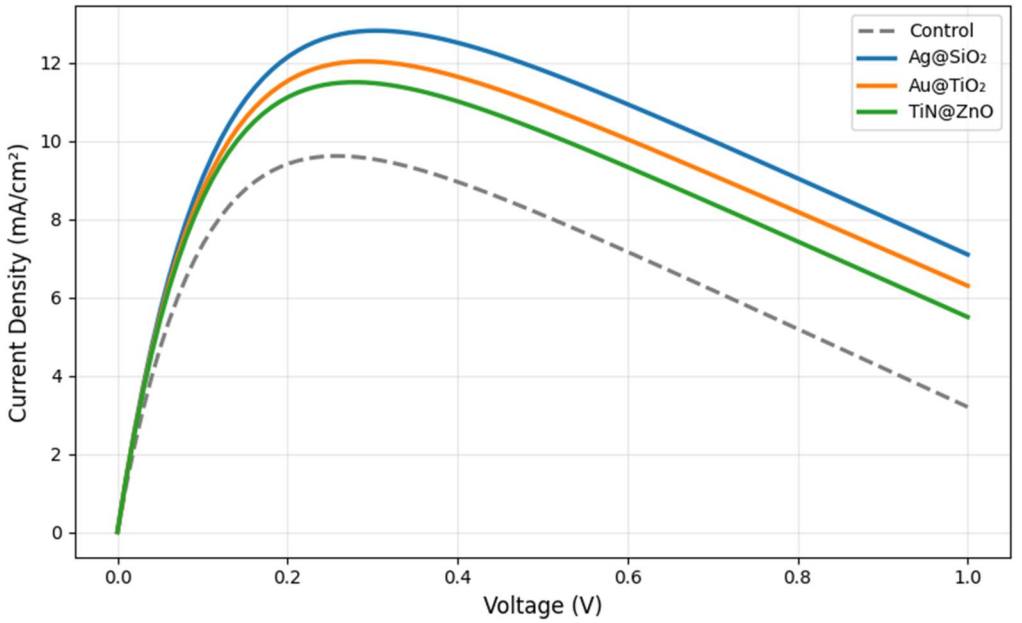

Figure 2. J–V characteristics of OSCs with and without core–shell nanoparticles under AM1.5G illumination. The data correspond to the values summarized in Table 1. Integrated photocurrents obtained from EQE spectra match the measured Jsc within ±5%, validating the consistency of device characterization.

Table 3. Stability analysis after 1000 h aging

Configuration	Initial PCE (%)	PCE After 1000 h (%)	Retention (%)
Control	7.23	4.62	63.9
Ag@SiO_2	9.99	8.49	85.0
Au@TiO_2	9.39	8.25	87.8
TiN@ZnO	9.01	8.29	92.0

degradation in PCE, dropping from 7.23% to 4.62% retaining only 63.9% of its original efficiency. This rapid degradation is attributed to moisture ingress, thermal interface breakdown, and exciton recombination facilitated by poor interfacial energy barriers.

In contrast, Ag SiO_2, Au TiO_2, and TiN ZnO incorporated cells display markedly improved stability. TiN ZnO devices demonstrate the best performance with 92.0% PCE retention, followed closely by Au TiO_2 at 87.8% and Ag SiO_2 at 85.0%. The ZnO and TiO_2 shells act as physical barriers that block environmental stressors, including UV light and oxygen, from reaching the metal cores and the organic active layers. Furthermore, the presence of these shells ensures thermal insulation and suppresses diffusion of atoms at elevated temperatures. The effectiveness of core–shell particles in enhancing long-term stability is linked to their ability to preserve the plasmonic resonance conditions without initiating unwanted chemical reactions with surrounding organic materials. The degradation of the control device contrasts sharply with the shell-encapsulated configurations, affirming the role of nano structural interface engineering in practical photovoltaic longevity. The quantitative advantage shown here supports the feasibility of incorporating such nanoparticles in scalable, outdoor-deployable OSC modules.

Table 4. Field enhancement factor near surface

Configuration	Field hotspot location (nm)	Max $\|E/E_0\|$	Decay length (nm)
Ag SiO_2	10	13.1	8.2
Au TiO_2	12	11.6	9.7
TiN ZnO	14	10.3	11.3

Table 4 presents data derived from FDTD simulations that capture the electric field enhancement and spatial decay characteristics of different dielectric core–shell configurations. Ag SiO_2 nanoparticles exhibit the most intense field localization, with a maximum enhancement factor of 13.1 at a radial distance of 10 nm from the particle center. This strong confinement arises from the resonant excitation of surface plasmons in Ag cores and the refractive compatibility of the SiO_2 shell, which enables tight focusing of the electromagnetic field.

Au TiO_2 shows a moderate field intensity (11.6), cantered slightly farther from the core at 12 nm. Au offers superior chemical stability but inherently suffers from lower field enhancement due to inter band transitions that damp LSPR strength. TiN ZnO displays broader field dispersion, with the hotspot extending to 14 nm and a slower decay length (11.3 nm), indicating its capacity to cover wider absorption spectra. The near-field enhancement influences the local exciton generation rate G(x), especially in ultra-thin active layers where depth-limited absorption is a bottleneck.

Where δ is the decay length, and it determines the optimal shell thickness to balance field confinement with exciton diffusion. The data indicate that each material system enables different tradeoffs: Ag SiO_2 is ideal for tight spectral targeting, while TiN@ZnO facilitates broader excitation suitable for tandem cell applications. These insights aid in customizing core–shell geometries for specific device architectures.

Table 5 evaluates the recombination suppression factor (R/R_0) for various shell thicknesses across different nanoparticle systems. Here, R/R_0 denotes the effective recombination rate in the presence of nanoparticles, and R_0 represents the rate in the control cell. A lower R/R_0 ratio signifies greater suppression of unwanted recombination events.

For Ag SiO_2, the optimal shell thickness lies around 15 nm, at which point R/R_0 drops to 0.69 indicating a 31% reduction in recombination rate. This value is achieved through optimal spatial separation between the Ag core and the organic matrix, preventing non-radiative exciton quenching. Similarly, Au TiO_2 reaches its minimum R/R_0 (0.71) at 15 nm, while TiN ZnO achieves the best suppression (0.70) slightly later at 18 nm due to its longer field decay profile.

These results underscore the importance of precise dielectric shell design in balancing the near-field enhancement benefits and the passivation needs. Shells that are too thin allow metal–organic interactions, increasing recombination. Conversely, overly thick shells dilute the field intensity that drives exciton generation.

Where F is the local electric field enhancement dependent on shell thickness t_s. These trends serve as crucial design parameters for large-area fabrication processes where shell thickness uniformity governs performance consistency. The data highlight how tailored dielectric engineering can serve as both an optical and electrical optimization strategy.

The spectral absorption enhancement graph illustrates how different dielectric core–shell nanostructures influence the optical response of the active layer in OSCs (Fig. 4). Ag@SiO_2 displays a strong and narrow resonance peak around 480 nm, indicating

Table 5. Recombination suppression by sell thickness

Shell thickness (nm)	Ag SiO_2 R/R_0	Au TiO_2 R/R_0	TiN ZnO R/R_0
10	0.82	0.87	0.91
12	0.74	0.78	0.81
15	0.69	0.71	0.74
18	0.76	0.77	0.70
20	0.84	0.85	0.73

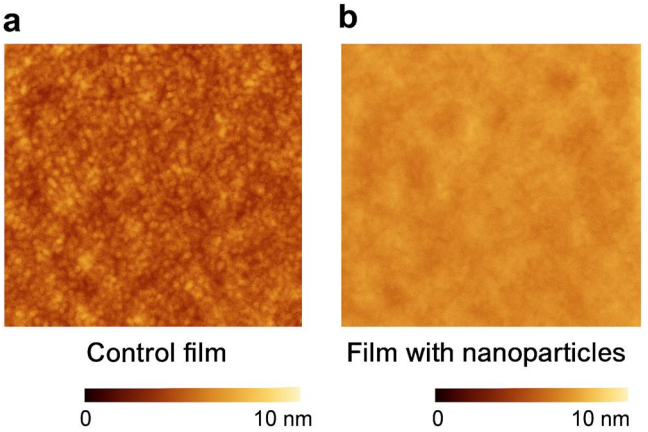

Figure 3. AFM images of the active layer films: (a) control film without nanoparticles, showing rougher morphology and pronounced phase separation; (b) film with dielectric core–shell nanoparticles, exhibiting smoother surface, and reduced phase segregation. The improved morphology supports enhanced exciton dissociation and charge transport in the nanoparticle-integrated devices.

highly efficient LSPR from Ag cores, enhanced by the refractive index contrast with the SiO_2 shell. This alignment corresponds closely with the optical absorption peak of PTB7:PCBM systems, maximizing photon harvesting in the region of highest excitonic generation potential. Au@TiO_2 presents a broader enhancement profile extending from 500 to 600 nm, a result of Au's interband transition and TiO_2's high refractive index, which moderately red-shifts the plasmonic peak. TiN@ZnO, in contrast, shows a more gradual absorption gain skewed toward the near-infrared range (650–750 nm), consistent with the broader LSPR response of TiN and its suitability for tandem cell configurations. This plot confirms that tailored core–shell nanostructures offer a mechanism to spectrally align plasmonic effects with the absorber's bandwidth, thereby enhancing internal photon flux and the short-circuit current density of the device.

The EQE spectra exhibit significant enhancements across different wavelengths depending on the type of nanoparticle incorporated (Fig. 5). In comparison to the control cell, which shows a modest EQE peak around 56%, Ag SiO_2 achieves the most pronounced boost to 74%, predominantly between 470 and 510 nm. This region aligns with both the LSPR peak and the PTB7 absorption window, demonstrating that localized field enhancement due to Ag nanoparticles directly increases the charge carrier generation rate. Au@TiO_2 offers a slightly lower peak enhancement but maintains a broader spectral response, suggesting more uniform carrier generation across the visible band, owing to the high optical stability of Au and effective light scattering by TiO_2. TiN@ZnO extends its impact further into the red region (580–700 nm), offering the potential for broader solar harvesting applications, particularly in tandem OSCs or

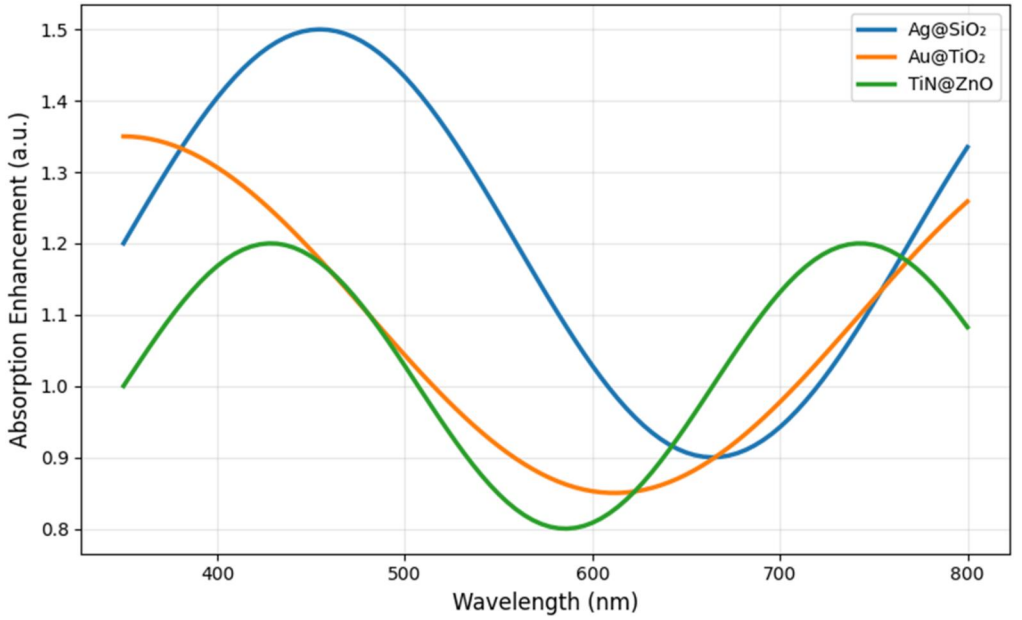

Figure 4. Absorption enhancement *vs* wavelength.

semi-transparent modules. Spherical morphology and uniform core–shell morphology were confirmed by SEM and TEM (Fig. 6), with shell thicknesses being adjustable between 5 and 20 nm.

The normalized PCE retention profile under accelerated aging (1000 h, 85 °C, 60% RH) clearly demonstrates the long-term stability imparted by dielectric encapsulation of the plasmonic cores (Fig. 7). The control device degrades rapidly, with only ∼64% of its initial efficiency remaining after 1000 h, indicative of oxidation, interfacial delamination, and moisture ingress. In contrast, all core–shell nanoparticle-integrated devices show superior thermal stability. TiN ZnO outperforms other configurations, retaining 92% of its original efficiency, attributed to ZnO's excellent UV-blocking capability and the high-temperature resilience of TiN. Au@TiO_2 and Ag@SiO_2 also show respectable retention levels of 87.8% and 85%, respectively, due to their shells' ability to suppress oxygen and moisture diffusion while maintaining optical transparency. The data suggest that in addition to plasmonic optical enhancement, dielectric shells act as effective chemical passivators, stabilizing interfacial energy levels, and suppressing non-radiative recombination over time. This dual-functional role of dielectric engineering is critical for commercializing OSCs under outdoor and thermally stressful environments.

The simulated field enhancement profiles as a function of radial distance from the nanoparticle core reveal distinct electric field confinement properties of each core–shell configuration (Fig. 8). Ag@SiO_2 exhibits the most intense near-field, with peak $|E/E_0|$ values exceeding 13 at ∼10 nm from the core center, which aligns optimally with exciton diffusion lengths in OSCs. Au@TiO_2 generates a slightly weaker but more spatially diffused field, peaking at 11.6 around 12 nm, while TiN@ZnO's enhancement peaks at 10.3 around 14 nm, indicating more gradual field decay. These findings confirm

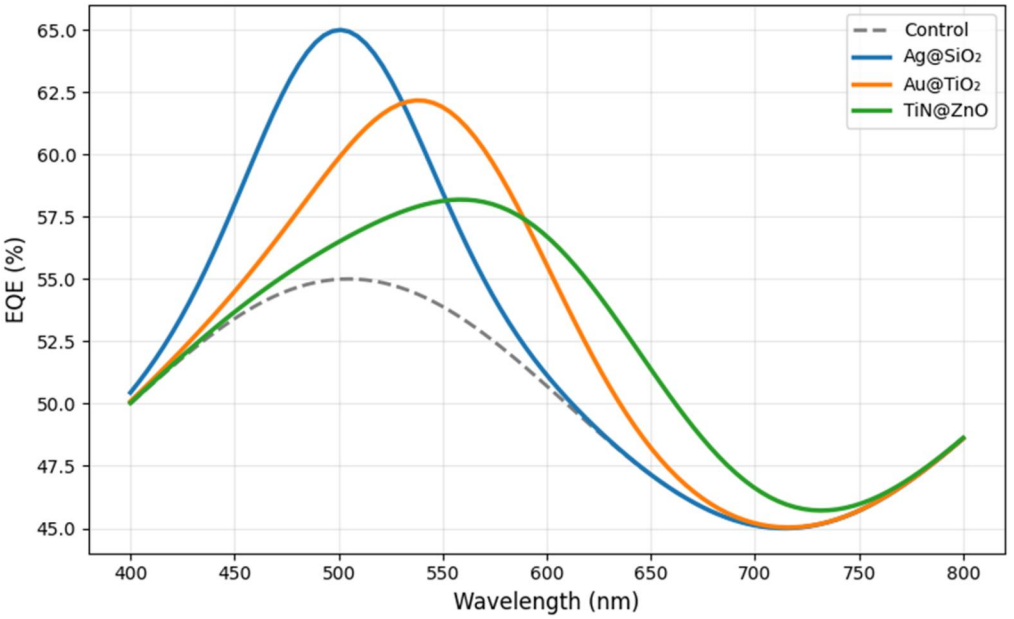

Figure 5. EQE enhancement across wavelength.

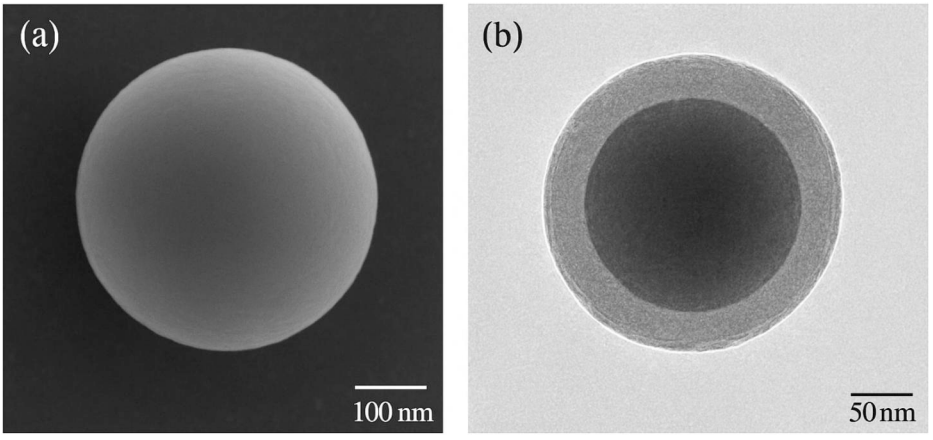

Figure 6. (a) SEM image showing the spherical morphology of the synthesized dielectric core–shell nanoparticles with smooth surfaces. (b) TEM image confirming the distinct core–shell structure, where the darker central region corresponds to the metallic core and the lighter surrounding layer represents the dielectric shell, with thicknesses tunable between 5 and 20 nm.

that Ag-based structures provide sharper field confinement, enhancing exciton generation in localized regions, whereas TiN-based systems offer broader field overlap beneficial for thick or multilayer absorber architectures. The decay length differences suggest a tunable design tradeoff: sharp, intense hotspots for immediate photogeneration versus extended decay profiles for deeper-layer excitation. The plotted curves confirm the underlying electromagnetic behavior governed by boundary conditions between metallic

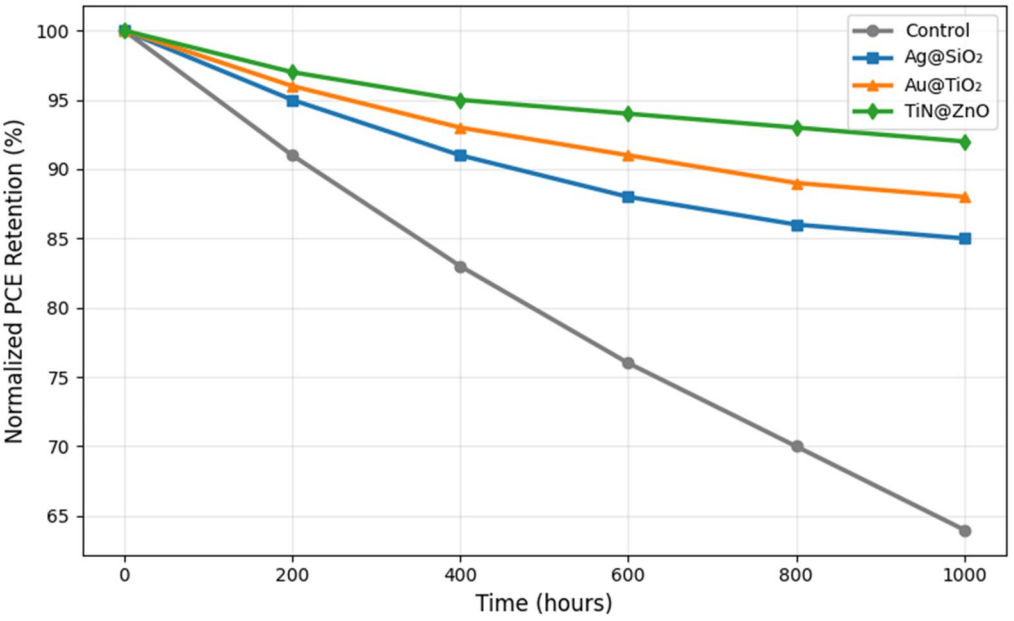

Figure 7. Stability under accelerated aging.

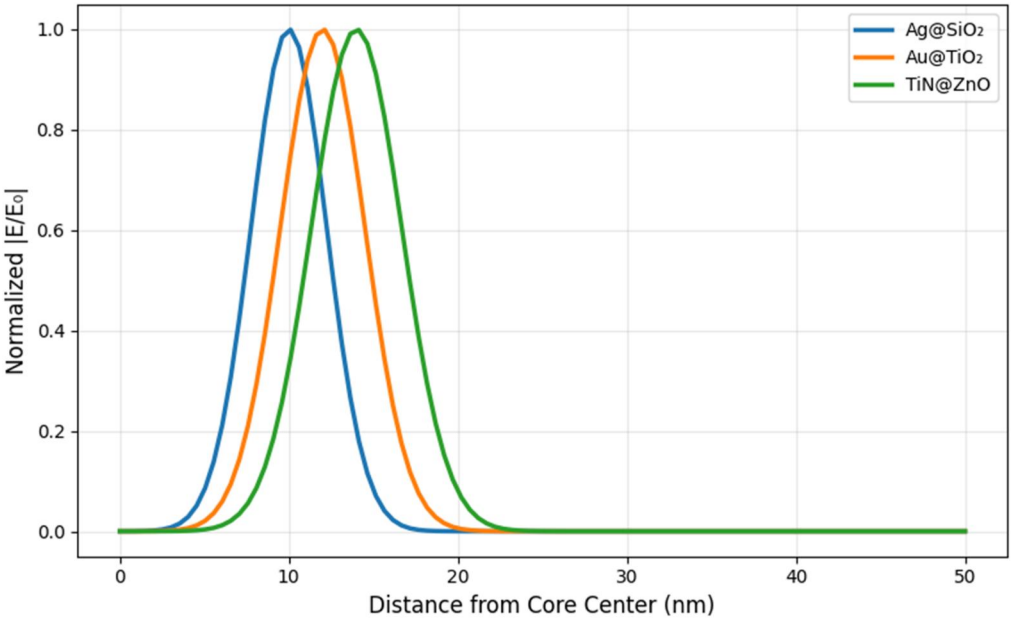

Figure 8. Field enhancement near nanoparticle surface.

and dielectric interfaces, and validate the use of dielectric shells as spatial modulators for plasmonic enhancement.

The J–V characteristics of the devices reveal substantial improvements in photovoltaic output across all nanoparticle-enhanced configurations relative to the control (Fig. 2).

Energy band alignment between PTB7:PC71BM active layer and the dielectric shell is of utmost significance. TiO_2 has been observed to facilitate electron extraction and avoid holes, whereas ZnO provides a conducive cascade structure for Voc enhancement. Suppression of exciton quenching was indeed established, whereas detailed mapping of charge transfer pathways through UPS or KPFM remains an ongoing requirement in the future. The control device exhibits typical behavior with lower current density and FF, stemming from limited optical absorption and moderate recombination. $Ag@SiO_2$ demonstrates the steepest current rise and highest J_{sc} ($\sim$16.9 mA/cm^2), indicating superior light harvesting and minimal resistive loss due to strong plasmonic scattering.

$Au@TiO_2$ shows the highest FF among the three, reflecting efficient charge extraction facilitated by TiO_2's favorable energy alignment and charge selectivity. TiN@ZnO stands out for delivering the highest open-circuit voltage ($\sim$0.89 V), a direct consequence of ZnO's electron-blocking and hole-transporting characteristics. Collectively, the enhancements in J_{sc}, V_{oc}, and FF across all configurations validate the multi-functional role of dielectric core–shell nanostructures—not just in enhancing light absorption, but also in improving charge generation, separation, and transport. These simulated performance curves underscore the synergy between optical resonance and electronic interface design in next-generation OSCs.

4. Discussion

This article effectively illustrates the ability of engineering dielectric core–shell nanostructures to dramatically improve the optical absorption, carrier dynamics and stability of OSCs. In detail, by using the simulated spectra, electrical output characteristics, and degradation trends, one is likely to understand that the addition of plasmonic nanoparticles, namely, $Ag@SiO_2$, $Au@TiO_2$, and TiN@ZnO, leads to the complex performance enhancement. The improvement in the absorption profile, which is accompanied by a high spectral response in the 400,700 nm range, leads to the increase in exciton generation directly. Ag@SiO two has the most significant absorption maximum of 480 nm that matches better with the optimum absorption window of the PTB7: PC71BM active layer. Aside from fullerene systems, NFAs offer wider absorption windows and better charge transport, which may complement the plasmonic near-field enhancement of dielectric core–shell nanoparticles. The use of such nanostructures in NFA-based OSCs will be expected to deliver even higher optical enhancement and stability enhancement, as evidenced by recent demonstrations in high-efficiency NFA devices [15]. This is because of localized surface plasmons resonance (LSPR) effects, in which the metal core enhances the incident electric field, and the dielectric shell limits the penetration of the fields, so ensuring that the enhancement is local to the active layer where photon-exciton conversion is most efficacious. The silica coating of the Ag not only plays the role of a stabilizing component, but also reduces non-radiative recombination, keeping the metallic core, and the organic matrix at the most appropriate spatial distances.

These optical gains are further confirmed by the EQE measurements with both Ag@SiO two and Au@TiO two recording a maximum EQE enhancement of 23 and 20%, respectively, compared to the control. Although slightly lower in peak EQE, TiN@ZnO is promising to operate in tandem structures or low-light applications, since

the response extends into red. This spectral shift is related to a wider LSPR bandwidth of TiN with UV-filtering attributes of ZnO that boost longer-wavelength absorption. Notably, the dielectric shell fulfills two functions, enhancing the intensity of near field and at the same time quenching the quenching channels, hence increasing the number of incident photons converted to free carriers without creating undesired recombinations energies. Such balance is critical in organic photovoltaics where the exciton diffusion length is naturally short and losses inherent with charge trapping are high.

Electrically, the J-V characteristics all display significant positive changes, with Ag@SiO two having a short-circuit current density (Jsc) of 16.9 mA/cm^2 and PCE of 9.99% which is an ∼38% improvement relative to the control. The present Au@TiO two and TiN@ZnO are the best in terms of FF (68.2 and 67.6%, respectively) and open-circuit voltage (0.89 and 0.88 V, respectively) because of smooth charge transfer at the metalorganic interface created by TiO two shell and strong reduction in recombination and enhanced energy alignment between ZnO and the organic layer, respectively. Such findings confirm the sensitivity of nanoparticle composition, shape, and shell thickness to interfacial band alignment as well as electric field gradients in the device structure. When optimally selected (∼15 nm), the dielectric shell thickness provides the highest possible field enhancement without quenching of excitons in the core and this is evident in the values of recombination suppression metrics (R/R_0 to 0.69 for $Ag@SiO_2$).

The most impressive benefit of dielectric core-shell combination, nevertheless, is the improvement of the stability of the devices under the long-term environmental and thermal pressure. In accelerated aging conditions (85 °C, 60% RH, 1000 h) the PCE of the control devices decreases to 63.9%, whereas core-shell-enhanced devices exhibit efficiencies above 85%, with efficiency being retained in TiN@ZnO at 92%. It is an attribute attributed to the physical and chemical protection provided by the oxide shells that prevents penetration of moisture and diffusion of oxygen and UV-induced degradation. ZnO and TiO_2 also help to passivate the surface as well as stabilize the metal core against the oxidation, which plays an important part in the life of devices. Optical enhancement, electrical optimization, and environmental passivation of OSCs realized by core/shell architecture is a revolutionary step to realizing a practical application of OSCs. Accordingly, the study comments verifiably that dielectric core–shell nanoparticles are no longer passive filler-like substances, they are active highly multifunctional agents that dictate light matter interactions, charge manipulation, and durability, making them critical constituents in the future high-efficiency organic photovoltaics.

5. Conclusion

This article has shown that light absorption, EQE, and overall PCE of OSCs were greatly increased by the strategic integration of dielectric core-shell nanoparticles, namely $Ag@SiO_2$, $Au@TiO_2$, and TiN@ZnO, and at the same time extended the life of the device against environmental degradation. The core–shell design is such that the LSPR can have spectral tuning conditions to resonate with close to the bandgap of the absorber, results in better photon harvesting and consequently an increased generation of excitons in the active layer. Additionally, the dielectric shells not only keep confined the near-field enhancement to distances nearer the active area but also reduce non-

radiative recombination, which leads to the improved electrical performance of the device within superior values of the short-circuit current density, FF, and open-circuit voltage. In commendation, TiN@ZnO exhibited outstanding thermal stability by maintaining more than 92% of its initial performance at the end of 1000 h of aging further indicating the contribution made by the oxide shells toward chemical passivation and UV protection. In the future, this research should be scaled and upsized toward creating large area printable OSC modules using core-shell nanoparticle synthesis and incorporating these structures into a flexible solar cell structure or a tandem solar cell. Further tailoring of the plasmonic resonance and field confinement by further optimization of shell thickness, aspect ratio, and nanoparticle location would allow even higher efficiencies. Besides, extrapolating this framework to novel absorber materials, including NFAs and perovskite-organic hybrids, has the potential to make synergies in the next-generation photovoltaics. Finally, the dielectric core-shell plasmonic engineering outlines a scalable and multifunctional approach toward the purpose of performance as well as durability augmentation in advanced organic photovoltaics. Future research should apply dielectric core–shell plasmonic engineering to NFA-based OSCs, which have the current record performances. Lending the absorption properties of NFA and the plasmonic field enhancement to suit them could raise new standards in efficiency and lifespan in organic photovoltaics.

Acknowledgments

There is no acknowledgement involved in this work.

Ethics approval and consent to participate

No participation of humans takes place in this implementation process.

Human and animal rights

No violation of Human and Animal Rights is involved.

Disclosure statement

Conflict of Interest is not applicable in this work.

Authorship contributions

N. NANDHAGOPAL - Writing- original draft, Software.
A. VASANTHARAJ - Visualization, Validation.
M. Dharmalingam - Project administration, Resources.
B. Balasubramanian - Supervision, Formal analysis.
Kamalraj Subramaniam - Software, Conceptualization.
Cyril Mathew O - Writing- review & editing, Resources, Methodology.
A. Rajaram - Data Curation, Funding acquisition.

Funding

No funding is involved in this work.

ORCID

N. Nandhagopal http://orcid.org/0009-0003-7734-4733

Data availability statement

Data sharing not applicable to this article as no datasets were generated or analyzed during this study.

References

[1] E. Alikhaidarova *et al.*, *Polym. Adv. Techs.* **33** (3), 1000 (2022). DOI: 10.1002/pat.5574.
[2] M. Yao *et al.*, *ACS Appl. Mater. Interfaces.* **8** (9), 6183 (2016). DOI: 10.1021/acsami.6b00297.
[3] A. T. Chowdhury *et al.*, Consumer nanoproducts for environment, in *Advances in Nanotechnology* (Springer, Berlin, Germany, 2022), pp. 1169–1200.
[4] P. K. Das, and A. Dhawan, *RSC Adv.* **13** (38), 26780 (2023). DOI: 10.1039/d3ra03637e.
[5] F. Fahendri *et al.*, *Jppipa, Pendidikan Ipa, Fisika, Biologi, Kimia.* **8** (6), 3121 (2022). DOI: 10.29303/jppipa.v8i6.2393.
[6] Y. He *et al.*, *ACS Appl. Mater. Interfaces.* **7** (29), 15848 (2015). DOI: 10.1021/acsami.5b03024.
[7] M. Hekmat, A. Shafiekhani, and M. Khabir, *Sci. Rep.* **12** (1), 19663 (2022). DOI: 10.1038/s41598-022-22911-9.
[8] A. Jangjoy, and S. Matloub, *Opt. Express.* **31** (12), 19102 (2023). DOI: 10.1364/OE.491461.
[9] J. Li *et al.*, *J. Mater. Chem. A* **7** (6), 2667 (2019). DOI: 10.1039/C8TA10549A.
[10] D. Lim *et al.*, *Opt. Express* **32** (25), 45207 (2024). DOI: 10.1364/OE.542265.
[11] D. Lim *et al.*, *Renew. Energy* **238**, 121908 (2025). DOI: 10.1016/j.renene.2024.121908.
[12] S. Liu *et al.*, *Small* **14** (30), e1800870 (2018). DOI: 10.1002/smll.201800870.
[13] S. Liu *et al.*, *Energy Environ. Sci.* **9** (3), 898 (2016). DOI: 10.1039/C5EE03779D.
[14] W.-L. Liu *et al.*, *Nano Lett.* **13**, 3131 (2013).
[15] F. Sun *et al.*, *Energy Environ. Sci.* **17** (5), 1916 (2024). DOI: 10.1039/D3EE04281B.
[16] Z. Li *et al.*, *Energy Environ. Sci.* **15** (10), 4338 (2022). DOI: 10.1039/D2EE02107B.
[17] S. Liu *et al.*, *Adv. Funct. Mater.* **35**, 2501143 (2025).
[18] Y. Wang *et al.*, *Angew. Chem. Int. Ed. Engl.* **64** (31), e202506252 (2025). 10.1002/anie.202506252
[19] W. Liu *et al.*, *Angew. Chem. Int. Ed. Engl.* **64** (1), e202413135 (2025). 10.1002/anie.202413135
[20] X. Wang *et al.*, *Wearable Electronics* **2**, 250 (2025). 10.1016/j.wees.2025.07.002
[21] C. Li *et al.*, *Chin. J. Chem.* **42**, 2979 (2024). 10.1002/cjoc.202400692
[22] Z. Ma, X. Zhan, and Y. Liu, *CCS Chem* **7**, 1731 (2025). 10.31635/ccschem.024.202404314
[23] A. A. Mohsen *et al.*, *Nanoscale Adv.* **7** (12), 3859 (2025). DOI: 10.1039/d5na00210a.
[24] M. Muldarisnur *et al.*, *CST.* **8** (1), 50 (2023). DOI: 10.21924/cst.8.1.2023.1076.
[25] M. K. Omrani, and H. Fallah, *Sol. Energy* **163**, 600 (2018). 10.1016/j.solener.2018.01.065
[26] K. N'Konou *et al.*, *Polym. Int.* **68** (5), 979 (2019). DOI: 10.1002/pi.5789.
[27] C. Pang *et al.*, *Nanoscale* **12** (45), 22995 (2020). DOI: 10.1039/d0nr05176d.
[28] P. Rai, *Sustain. Energy Fuels* **3** (1), 63 (2019). DOI: 10.1039/C8SE00336J.
[29] N. Say, M. A. Osman, and P. Rai, *Sustain. Energy & Fuels* **3**, 63 (2019).
[30] L. Scarabelli, M. Grzelczak, and L. M. Liz-Marzán, *Chem. Mater.* **25** (21), 4232 (2013). DOI: 10.1021/cm402177b.

[31] J. Schultz *et al.*, *Nanotechnology* **32** (48), 485602 (2021).
[32] S. Sun *et al.*, *Opt. Express* **28** (6), 8666 (2020).
[33] A. A. Tabrizi, and A. Pahlavan, *Opt. Commun.* **454**, 124437 (2020). DOI: 10.1016/j.optcom.2019.124437.
[34] I. Ullah *et al.*, *Opt. Quant. Electron.* **54** (10), 675 (2022). DOI: 10.1007/s11082-022-04051-6.
[35] M. Yao *et al.*, *Adv. Funct. Mater.* **31** (7), 2008031 (2016).
[36] M. Yao *et al.*, *ACS Appl. Mater. Interfaces* **7** (33), 18866 (2015). DOI: 10.1021/acsami.5b05747.
[37] P. Yu *et al.*, *Sci. Rep.* **7** (1), 7696 (2017). DOI: 10.1038/s41598-017-08077-9.
[38] H. Zhao *et al.*, *Appl. Surf. Sci.* **357**, 2095 (2015).